Faculté de physique et ingénierie
Université de Strasbourg

master Physique Subatomique Astroparticules

Master Science, Mention Physique
Spécialité Physique Subatomique et Astroparticules

Année universitaire **2019-2020**

Aurélien GIRY

NUCLEAR OBSERVABLES FOR ASTROPHYSICS PROCESSES

Rapport de stage de Master
sous la direction de Kamila SIEJA

2 Mars 2020 au 30 Juin 2020

IPHC Institut Pluridisciplinaire Hubert CURIEN STRASBOURG

Université de Strasbourg

Abstract

The field of nuclear astrophysics is an interdisciplinary field at the crossroads of astrophysics and nuclear physics. It aims to answer fundamental questions of the origins of the elements in the universe and to tackle nuclear reactions in physics of stellar objects. We will focus on the r-process, which forms about half of the elements with a nucleon number $A > 70$.
A key component in the r-process is the cross section for radiative neutron capture. Theoretical predictions of these cross sections are required and one needs radiative strength function to use the statistical model. The major contributions to the RSF come from $E1$ and $M1$ transitions with small additions of $E2$ transitions. They are usually parameterized by a Lorentzian which is motivated by the success of describing the electric giant dipole resonance by such a form. While it is successful for the description of collective nuclear excitations, deviations from this behavior were found at the lowest transitions energies, where e.g. an enhancement for $M1$ transitions was observed. The calculations of neutron capture cross-section are often performed in the Hauser-Feshbach model which relies upon the assumption, known as the Brink-Axel's hypothesis, that the strength function is independent of the considered state.
This internship will focus on calculations of the radiative strength function for $M1$ and $E2$ transitions for nuclei around $A \approx 50$, most notably ^{48}Cr, ^{48}Ti and ^{50}Ti. We will delve on the validity of the Brink-Axel's hypothesis for these nuclei by looking at the effects of applying cuts in excitation energies on the states in the calculations on the global shape of the radiative strength function. If the Brink-Axel's hypothesis was fulfilled, it should be invariant. We will also study the influence of the shape of the nucleus upon the presence or not a low energy enhancement at low energies in the radiative strength function. More precisely, ^{48}Ti is a spherical nucleus whereas ^{48}Cr is deformed and ^{50}Ti is a semimagic nucleus.

Résumé

Le domaine de la physique nucléaire est un domaine interdisciplinaire à la croisée des chemins entre l'astrophysique et la physique nucléaire. Son but est de répondre à des questions fondamentales sur l'origine des éléments dans l'univers et d'adresser les réactions nucléaires dans la physique des objets stellaires. Nous nous concentrerons sur le processus r, qui forme environ la moitié des éléments avec un nombre de nucléon $A > 70$.
Une information clé en astrophysique nucléaire est la section efficace de capture radiative de neutron. Les prédictions théoriques de ces sections efficaces sont requises and il est nécessaire d'avoir les fonctions de transert radiatif pour utiliser le modèle statistique. Les contributions majeures proviennent de transitions $E1$ et $M1$ avec de faibles additions de transitions $E2$. Elles sont en général paramétrisés par une lorentzienne, ce qui est motivé par le succès dans la description de la résonance électrique géante d'une telle forme. Bien que cela soit une réussite pour les descriptions des excitations nucléaires collectives, des déviations de ce comportement ont été trouvées aux transitions d'énergies les plus basses i.e. une augmentation pour les transitions $M1$ ont été observées.
Les calculs sont en général faits dans le cadre du modèle d'Hauser-Feshbach lequel repose sur la supposition, connue comme l'hypothèse de Brink-Axel, que la fonction de force est indépendante de l'état considéré.
Ce stage se concentra sur les calculs de fonction de transfert radiative pour des transitions $M1$ et $E2$ pour des noyaux avec $A \approx 50$, plus précisément ^{48}Cr, ^{48}Ti et ^{50}Ti. Nous nous concentrerons sur la validité de l'hypothèse de Brink-Axel pour ces noyaux en s'intéressant aux effets qu'ont des coupures en énergie d'excitations sur les états dans les calculs pour la forme globale de la fonction de transfert radiatif. Si l'hypothèse de Brink-Axel est vérifée, alors elle devrait rester invariante. Nous étudierons également l'influence de la forme du noyau sur la présence ou non d'une augmentation à basse énergie de la fonction de transfert radiatif. Plus précisément, ^{48}Ti est un noyau sphérique alors que ^{48}Cr est déformé et ^{48}Ti est un noyau semimagique.

Contents

1 Introduction

This internship was performed between the 2 March 2020 and the 30 June 2020 at the Institut Pluridisciplinaire Hubert Curien in Strasbourg in the Theory Group. The goal of this internship was to investigate the Radiative Strength Functions (RSF) of different multipolarities and type for different nuclei. RSF are a key component in astrophysical calculations. The Quasiparticle Random Phase Approximation (QRPA) formalism offers a model which is currently the only one to work for all nuclei. This approach has been developed for example in Ref. [7]. It has shown to yield results in pretty good agreement for the RSF when free parameters are added such as in Ref. [8]. Those parameters are adjusted thanks to RSF calculations done with the Shell Model, which will be the framework used in this internship. Usually, RSF are approximated by Lorentzian but effects such as an enhancement at low energies underlines effects that are not captured by this simple formula. More precisely, Lorentizan mostly fails to describe an increase of the dipole (multipolarity $L = 1$) strength below 3 MeV γ-ray energy which has been found in several nuclei in the mass range $A \approx 50 - 100$ in experiments.
There have been numerous Shell-Model based theoretical studies as in Refs. [9] and [10]. Shell-model calculations have been able to probe that an enhancement at low-energies for the $M1$ strength function is a common feature for numerous nuclei. Ref. [12] also highlights that the Brink-Axel hypothesis is well checked at higher excitation energies for nuclei around the $N = 82$ shell closure. This behavior can be explained by radiation from many close-lying states of a similar structure in nuclear quasi-continuum.
Regarding $E1$ calculations, Ref. [11] shows, using the Shell Model, that there is no enhancement at low energies for ^{44}Sc. This conclusion holds for neighboring nuclei. It also produces an enhancement at low energies for the $M1$ RSF. Finally, the sum of theses contributions have been shown to reproduce experimental date pretty well for excitation energies in the range $4 - 8$ MeV, within the error bars range of the experimental data. For lower energies, the magnetic part fits with the error bars with the experimental data.
Some SM calculations have also been done for $E2$ transitions. Notably, $E2$ transitions have been studied for ^{94}Mo and ^{95}Mo in Ref. [14]. It has shown the domination of the large number of transitions between $J_f = J_i$ with $J_i = \pm 1$ of the distribution of the average $B(E2)$. The deduced strength functions increase toward zero transition energy and show a finite Gauss-shaped maximum. This is a very different behavior than the phenomenological expression recommended in the reaction data base RIPL [15]. Also in an energy range up to about 6 MeV, the average $E2$ strength function calculated with the Shell Model is greater than the phenomenological expression by one order of magnitude.
While the enhancement of the $M1$ transitions have been found in several nuclei, there are neighboring nuclei were no such enhancement has been observed. For example, titanium and chromium nuclei have been previously studied in [13]. It is shown that while nearly all the titanium isotopes have an upbend in their strength function for $M1$ transitions, no such upbend is present in the chromium, up to ^{51}Cr. Most notably, ^{48}Cr is an example of a prolate-deformed rotor in the pf-shell as was shown in Ref. [16]. Systems with such deformation have been shown not to have an upbend at the lower energies but instead the RSF is rather flat towards $E_\gamma = 0$. This indicate that the shape of the nucleus plays a role in the presence of the upbend at low energies for $M1$ transitions. In this study, we are going to investigate the properties of $M1$ and $E2$ transitions for ^{48}Cr, ^{48}Ti and ^{50}Ti, most notably their radiative strength function and their yrast lines. $E2$ transitions have not been studied previously for theses elements. These nuclei can be studied in the pf shell and therefore there is only the positive parity to consider. Having the same mass, ^{48}Ti is a spherical nucleus while ^{48}Cr is deformed. ^{50}Ti is an example of a semi-magic nucleus (N=28).
We will first recall the properties of nuclear reactions and nuclear decays which lead to multiple hypothesis on the RSF themselves. Next we will describe the nuclear structure model used to calculate numerically the states and the transitions for a given nucleus. Then we will investigate the properties of γ-ray transitions which enter the calculations of the RSF. Following this we will examine the results obtained with the code developed during the internship. We will examine the RSF of the mid-mass nuclei $A \sim 48$ with a special emphasis on the $E2$ transitions, examine the possible dependence of the $E2$ RSF on the shape of the nucleus and examine the validity of the Brink-Axel hypothesis for the

studied cases.

2 Nuclear reactions & Nuclear decays

2.1 The field of nuclear Astrophysics

Nuclear astrophysics is the interdisciplinary field within physics merging the physics of large-scale objects (astrophysics) and of small-scale objects (nuclear physics). Its goal is to describe the processes occurring in the universe and their effects on its evolution. A key topic in nuclear astrophysics is the **Nucleosynthesis**. This term covers all the processes that create the elements in our universe and the influence of the astrophysical conditions on the properties of these processes.
It can be classified into three subgroups :

- Big bang nucleosynthesis : The first nucleosynthesis, which happened in the first minutes after the Big Bang, is responsible for the creation of the lightest nuclei : Hydrogen and Helium, which have been the fuel for the first stars.
- Stellar nucleosynthesis : There are two processes : the pp-chain which leads to the creation of Helium and the CNO cycle. This cycle burns lighter elements from Helium to Carbon, Neon, Oxygen up to Silicon for the heaviest stars.
- Explosive nucleosynthesis : Those are the processes occurring under extreme conditions such as neutron stars mergers or supernovae explosions.

The last process is the one responsible for the creations of most of the nuclei in the Segré chart. It leads to the creation of heavy elements, which are made by capture of neutrons and as such there is a need to determine the neutron capture cross section in radiative reaction. This process can be subdivided into two, depending on the neutron density :

- **s-process :** Occurring at small neutrons densities (time-scales of neutron captures are slow compared to those of beta-decay). It follows the valley of stability and thus explains the abundance of magic number nuclei.
- **r-process :** Occurring at large neutron densities and at high temperatures. It creates about half of $A \approx 60$. It follows an isotopic chain until a $(n,\gamma) \Longleftrightarrow (\gamma,n)$ equilibrium where we note $(n,\gamma) : A + n \rightarrow B + \gamma$

The r-process proceeds up to nuclei characterized by a longer lifetime : the waiting point nuclei, where it stops until a β-decay occurs. Such nuclei are the magic neutron shell closures where the (n,γ) reaction rate drops which explains the longer lifetime of such nuclei. The r-process runs through isotopes with extreme neutron excess which can not be synthesized in experimental facilities, hence we need theoretical predictions of the neutron capture cross sections which are usually performed in the **Hauser-Feshbach** model. The main classification of nuclear reactions is usually done according to the reaction time-scales, fast being reaction time comparable to fly-by time if both reaction partners would not interact (scattering process).
Let's consider a reaction $A + a \rightarrow B + b$, then the Q value is defined by : $Q = m_a + m_A - (m_b + m_B)$. It is the energetical possibility of a reaction. Here the masses are the nuclear masses (the atomic masses including the nuclear masses and the binding energies of the electrons). If Q is positive, then the reaction is permitted, otherwise it is not energetically allowed.

2.2 Compound nucleus (CN)

We now consider a nuclear reaction where the bombarding particle loses all its energy to the target nucleus and becomes an integral part of a new, highly excited, unstable nucleus. We called this resulting nucleus made of the incident particle and the target nucleus which are indistinguishable, the compound nucleus (CN). The basic assumption is that the formation and the decay of the compound nucleus are independent of each other.

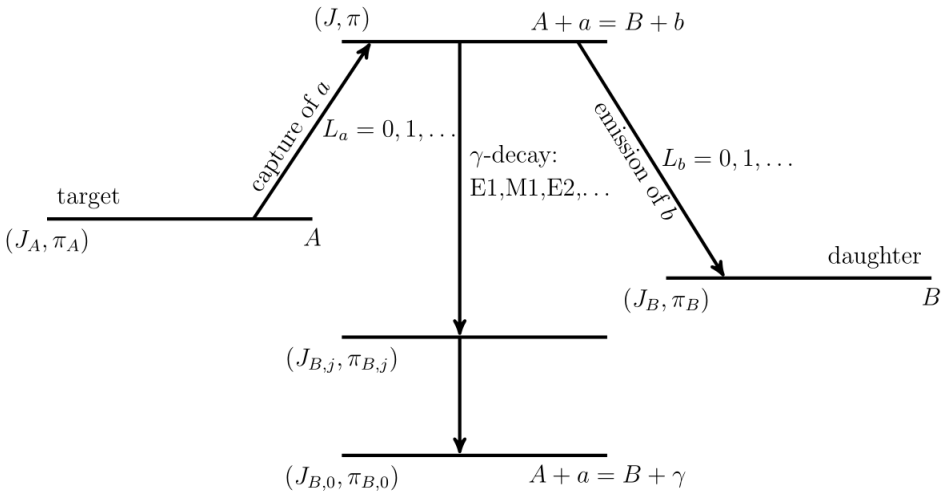

Figure 1: Scheme of a Hauser-Feshbach reaction, ie. $A + a \rightarrow$ highly excited compound nucleus $\rightarrow B + b$, taken from Ref. [1]

The formation stage takes a period of time approximately equal to the time interval for the bombarding particle to travel across the diameter of the target nucleus (about 10^{-21} second). Secondly, after a relatively long period of time (typically from 10^{-19} to 10^{-15} second) and independent of the properties of the reactants, the compound nucleus disintegrates, usually into an ejected small particle and a product nucleus.
For the compound nucleus, peaks in the cross-section are typical. Each peak is manifesting a particular compound state of nucleus. Theses peaks and the associated compound nuclei are usually called resonances.
If a CN is formed, then we can consider the energy of the incident neutron to be shared uniformly between all the nucleons before the deexctitation of the system by gamma or particle emission. This can be justifies due to the level density in the compound nucleus being high enough to ensure an average statistical continuum superposition of available resonances, ie. there is no distinguished state on which the neutron is captured.

2.3 Hauser-Feshbach model

The large number of nucleons and the high excitation energies leads to many accessible states. The Hauser-Feshbach (HF) model is a theoretical formulation of the compound nucleus picture. This is a model using statistical averages over the resonances instead of a single resonance model.
Figure 1 shows the principle schematics of a CN reaction. Due do the conservation laws arising from an electromagnetic transition we have the following conservation laws:

$$E = E_A + E_a - Q \tag{1a}$$

$$|J_A - l - s_A| \leq J \leq J_A + l + s_A \tag{1b}$$

$$\pi = (-1)^l \pi_A \pi_a \tag{1c}$$

Here we have noted the angular momentum J, the orbital angular momentum l and the spin s and as such we have $J = l+d$ More generally, for an X-type electromagnetic transition and an L-multipolarity, we have the following laws for the angular momentum and the parity π :

$$|J_A - l| \leq J \leq J_A + l \tag{2a}$$

$$\pi = (-1)^L \pi_A \text{ (X=electric)} \tag{2b}$$

$$\pi = (-1)^{L-1} \pi_A \text{ (X=magnetic)} \tag{2c}$$

This has been written for the projectile, for the decay nucleus, we can replace A by B and a by b to have the selection rules for the decay nucleus.

2.4 The model

Due to the Bohr's hypothesis underlying the CN reaction (independence between the formation and the decay of the CN), the cross section can be factorised into two parts : one for the formation and one for the decay probability. We now introduce **reaction channel** which specifies the particles as well the quantum numbers involved. For example, the γ-channel describes all possible γ-decays that might occur for a given compound nucleus.
As shown in Ref. [2], the (n,γ) cross-section at the center-of-mass energy E is proportional to :

$$\sigma^{\mu\nu}_{(n,\gamma)}(E,n) \propto \sum_{J,\pi}(2J+1)\cdot\frac{T^{\mu}_{n}T^{\nu}_{\gamma}}{T^{\mu}_{n}+T^{\nu}_{\gamma}} \tag{3}$$

where J is the half-integer neutron spin, T^{μ}_{n} and T^{ν}_{γ} are transmission coefficients i.e. the probability of penetration of the potential barrier. In astrophysics applications, the incident neutron energy is of the order of the keV which leads to $\sigma^{\mu\nu}_{(n,\gamma)}(E_i,n) \sim T^{\nu}_{\gamma}$.
The transmission coefficient for a photon of energy E_γ for a state μ in a given X-type, L-multipolarity transition is given by the following relation in terms of the RSF f_{XL}:

$$T^{\mu}_{\gamma}(E,J,\pi^{\mu},E,J,\pi) = T_{\gamma}(E_\gamma;XL) = 2\pi f_{XL}(E_\gamma)E^{2L+1}_{\gamma} \tag{4}$$

This will be studied later in 4.3.

3 Nuclear structure model

3.1 Nuclear level densities

Let $N(E)$ be the number of levels up to an energy E. The nuclear level density (LD) is defined as :

$$\rho_{nucl}(E) = \frac{N(E+\Delta E)-N(E)}{\Delta E} \xrightarrow{\Delta E\to 0} \frac{\mathrm{d}N}{\mathrm{d}E} \tag{5}$$

The LD have a large influence on Hauser-Feshbach predictions because of its exponential rise, thus it is an important quantity for this model. The basic assumption of HF is the existence of a reasonably large number of overlapping resonances. That is why the application of this model for magic nuclei is problematic because these nuclei exhibit small LD due to the shell gap. The same concerns light nuclei.
The basic approach is to count the number of levels in the needed energy interval, ie. compute all the eigenvalues of the nuclear Hamiltonian and their degeneracy and then count how many fall into the interval $[E, E+\mathrm{d}E]$. As an example, if the nucleus is in its ground state, all levels are filled up to the Fermi level. If the nucleus is excited, then fermions can be excited to a level above the Fermi level. The places where the particles stood are the hole-states, the places where the particles are present are the particle-states.
The more energy there is, the more states above the Fermi level are available.

3.2 Nuclear Hamiltonian problem

Because derivations of nuclear interactions from QCD are still ongoing, we consider microscopic models which employ phenomenological interactions. The microscopic Hamiltonian H in a non-relativistic model in which we assume that only two-body interactions are relevant takes the following form :

$$H = \sum_{ij} t_{ij}a^{\dagger}_{i}a_{j} + \frac{1}{4}\sum_{ijkl}\bar{v}_{ijkl}a^{\dagger}_{i}a^{\dagger}_{j}a_{l}a_{k} \tag{6}$$

Where the indices i, labeling single-particle states, goes from 0 up to ∞. The $\bar{v}_{ijkl}$ are the antisymmetrized matrix elements of the two-body interaction. We ought to diagonalize this Hamiltonian but in practice it is impossible because the Hilbert space is of an infinite dimension, thus we need to trim it. One can consider two options :

- Restrict the number of particles and states (1)
- Approximate the eigentstates of H by simpler wave functions (2)

We will concentrate on the first approach, the Shell-Model formalism, which was used for the results of this work. The second approach being known as Hartree-Fock.

3.3 Nuclear Shell Model

There are experimental evidences for shell structure, most notably, the magic numbers and single particle states. In our problem, compound nucleus reactions occur at relatively high excitation energies where many collision are not Pauli blocked. At lower energies, collisions tends to be Pauli suppressed and thus single-particle motion can persist. This means that instead of considering the interaction of one nucleon with all the others, we can consider this nucleon is only affected by an average potential. Such a potential has been empirically derived by introducing a spin-orbit into a harmonic oscillator mean field :

$$U(r) = \frac{1}{2}m\omega^2 r^2 + D \cdot \vec{l}^2 - C \cdot \vec{l} \cdot \vec{s} \tag{7}$$

We thus have : an isotropic harmonic oscillator potential, an orbit-orbit term and the spin-orbit coupling needed to reproduce the magic numbers (2, 8, 20, 28, 50, 82, and 126 being the first seven ones). This leads to single-particle levels splitting.
Using Wick's theorem, with a defined core as the reference state to the general nuclear Schrödinger equation, we obtain :

$$H = E_0 + \sum_i \epsilon_i : a_i^\dagger a_i : + \frac{1}{4}\sum_{ijkl} \bar{v}_{ijkl} : a_i^\dagger a_j^\dagger a_l a_k : \tag{8}$$

$: a^\dagger b :$ designates the normal ordering of the operators $a^\dagger$ and b, the ϵ_i are the single-particle energies obtained from a mean field. Thus the last term is a two-body term : the residual interaction. This is the part that contains everything which goes beyond the mean-field and this is this term that differentiate Hartree-Fock based methods from SM.

3.4 The Large Scale Shell Model

In this approach, we sunder the complete shell model of a nucleus into three parts :

- The inert core which is composed of the orbits that are always full. They all have an energy which is under the Fermi energy.
- The valence space which is the part where we allow nucleon excitation.
- The external space which is composed of the orbits that are always empty, therefore, there is no allowed excitations here.

Afterwards, we need to define a **valence space**, which is the basis for the calculations, an **effective interaction** which is designed for the valence space and a numerical method to diagonalize the Hamiltonian.
Ideally, one would need all the shells generated by the nuclear potential. As it leads to an infinite Hilbert space, we solve the problem in the valence space by using an effective interaction. Thus we trim the Hilbert space in such a way that low-energy shells are removed. This approximation is valid up to excitation energies of the nucleus which are not too high. By doing this approximation we got from a matrix element $\langle\psi| H |\psi\rangle$ to an effective matrix element $\langle\psi_{eff}| H_{eff} |\psi_{eff}\rangle$.
An often-used basis is the m-scheme which is built from all Slater determinants constructed from all possible configurations that the chosen valence space allows. The physical states are obtained by simply diagonalizing the Hamiltonian matrix $\langle\phi_{SD,\alpha}| H_{eff} |\phi_{SD,\beta}\rangle$.
This induce to use for quantum numbers the projections J_z and T_z. The dimensionality becomes : $d = \binom{d_n}{n}\binom{d_p}{p}$ where d_n is the degeneracy of the neutron space, d_p the degeneracy of the proton space, n is the number of neutrons in the valence space and p is the number of protons in the valence space.

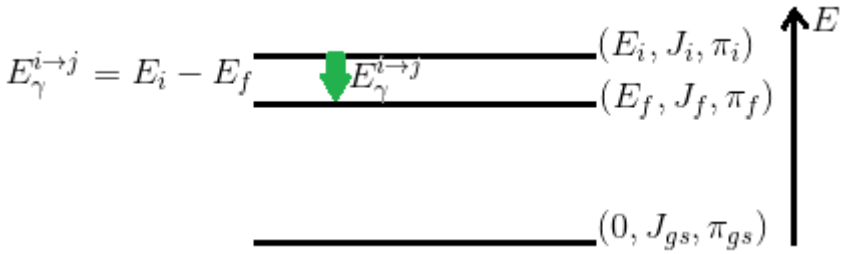

Figure 2: Scheme of a γ-transition

4 γ-ray transitions in nuclei

4.1 Electric and magnetic transitions

Let's consider two states, i and j, respectively at the excitation energy of E_i and E_f. The only deexcitation which conserves the number of protons and neutrons is the emission of γ-rays, which are carried by the electromagnetic force. The energy of the corresponding transition from the initial state i to the final state f is $E^{i\to j} = E_i - E_f$, as shown on figure 2. γ-rays are characterized by their type X (electric or magnetic) and the momentum L they carry.
Electric-type transitions are represented by the Q_L operator, whereas magnetic-type transitions are represented by the M_L operator.
From which arise the reduced transitions probabilities for an X-type transition of multipolarity L :

- $B(EL, J_i \to J_f) = \frac{1}{2J_i+1} |\langle f| |Q_L| |i\rangle|^2$
- $B(ML, J_i \to J_f) = \frac{1}{2J_i+1} |\langle f| |M_L| |i\rangle|^2$

The name reduced comes from the absence of any angular momentum information. The selection rules are the following : $|J_i - J_f| \leq L \leq J_i + J_f$ for the angular momentum and $\pi_i = (-1)^L \pi_f$ or $\pi_i = (-1)^{L+1} \pi_f$ for the parity for electric transitions (respectively for magnetic transitions). The change of parity for L=1,2 and 3 is summarized in Table 4.1 :

Table 1: The behavior the three first multipolarities for both electric and magnetic type transitions

Type \Multipolarity	1	2	3
Magnetic	No	Yes	No
Electric	Yes	No	Yes

4.2 Rotational Bands

4.2.1 Rotational motion

Rotational motion is guided by deformation of multipolarity $L = 2$ which are the quadrupole deformations, the collective phenomena which are excitations in which a large number of nucleons, even all nucleons, participate. They mostly occur at high energy while single-particle excitations occurs at low-energy. In particular, giant resonances are collective excitation involving all nucleons. They present a large magnitude of the resonance and they can be parametrized with a Lorentzian form factor. However this does not apply for low energies. In the case of the quadrupole deformations, they yield either prolate or oblate nucleus for a spherical shape nucleus. This is represented on Fig. 3. We will now consider the rotational energy by following the steps of Ref. [4]. The classical expression for the rotational energy is :

$$H = \sum_{i=1}^{3} \frac{R_i^2}{\mathcal{J}_i} \tag{9}$$

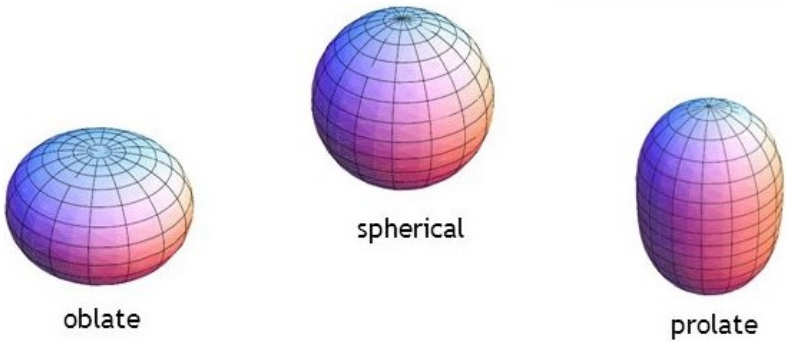

Figure 3: The three shapes a nucleus can take

Where R_i is the angular momentum generated by the motion of the nuclei and $\mathcal{J}_i$ are the moments of inertia. Now, if we take the Hamiltonian in the frame of quantum mechanics, then its eigenvalues form regular sequences, which are the rotational bands.
Following the steps of [5] we can consider the nucleus as a droplet of quantum liquid where its shape is a consequence of the shell structure. A deformed nuclear surface specifies an orientation in space and as such it can perform a quantal rotation. That is, a rotor Hamiltonian of type 9 describes this excitation mode, which carries the ''collective'' angular momentum $\vec{R}$. If we consider a quadrupole deformation of a nucleus of moment inertia $\mathcal{J}$, we can note that the ratio $\mathcal{J}/B(E2)$ is nearly constant because both the numerator and the denominator are proportional to the square of the deformation parameter. As such it is often seen as an evidence of a correlation between these two parameters.

4.2.2 Magnetic Rotation

Experimental results show that nuclear rotation is not a collective phenomenon that occurs only in well deformed nuclei. The reason is that the ratio is very large for the dipole bands in comparison to the same ratio for well deformed heavy nuclei and superdeformed nuclei. This leads to the conclusion that something has to carry a long transverse magnetic dipole moment but almost no charge quadrupole moment.
We can interpret this open question in the following way : high-j protons particles and neutron holes form current loops embedded in the mass distribution of the nucleus, which is nearly spherical.
These loops are associated with transverse magnetic moment μ_T and we can specify as such an angle of rotation around the axis **J**.
We can associate with protons particles an angular momentum $\vec{j_p}$ and with neutron holes an angular momentum $\vec{j_n}$. To increase the total angular moment $\vec{J}$, one have to align the angular momenta $\vec{j_n}$ and $\vec{j_p}$. This mechanism is called the shears arrangement. This name comes from the resemblance of the motion with the closing of a pair of a shears, which have a spring to keep them open. The dipole bands are thus referred to as shears bands. The shears arrangement of the high-j orbitals gives rise to a large transverse magnetic dipole moment. It is this long transverse dipole that rotates and generates the strong magnetic radiation. Ref. [6] called it the "magnetic rotation". (This name is a reference to the order parameter that specifies the orientation).
If we close the two blades of the shears, then the transverse component of the magnetic moment becomes shorter. This leads to the decrease of the $B(M1)$ values with increasing angular momentum as an inevitable consequence of the shears mechanism. This is summarized on figure 4.

4.3 Radiative strength function

As seen in 2.4, the transmission coefficient is directly linked to a function f_{XL}, the radiative strength function, which depends on the type of transition X, the multipolarity L and the energy E_γ. Let us consider a γ-decay from an initial level a to a final level b. The relevant quantum numbers for a level i being (E_i, J_i, π_i). There are two parametrizations, whether with the transmission coefficient $T^\gamma_{ab}(XL)$

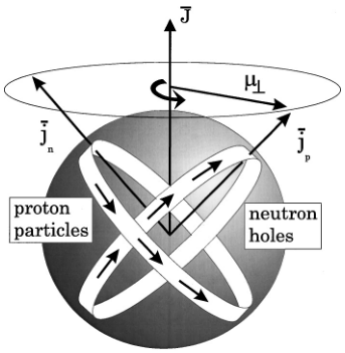

Figure 4: The shear mechanism. The angular momenta of the protons $\vec{j}_p$ and of the neutron holes $\vec{j}_n$ are separately lined-up. If they got aligned then the total momentum $\vec{J}$ will get larger.

or with the partial width : $\bar{\Gamma}^{\gamma}_{ab}(XL)$

$$2\pi E_{\gamma}^{2L+1} f_{XL} = T^{\gamma}_{ab}(XL) = \frac{2\pi}{D(E_a, J_a, \pi_a)} \bar{\Gamma}^{\gamma}_{ab}(XL) \tag{10}$$

The transition from an initial state to a final state and the transition from this final state to the initial state are related by a relation known as the principle of detailed balance which gives a relation between the reduced probability transition elements : $(2J_i + 1)B(XL, i \to f) = (2J_f + 1)B(XL, f \to i)$.
If we wanted to have such a relation for the respective RSF, we would need the statistical distribution of the reduced matrix elements with respect to the energy. Hence in a first approximation we shall do the distinction between the **absorption** RSF $\overrightarrow{f}$ and the **emission** RSF $\overleftarrow{f}$.
The RSF for a X-type, L-multipolarity is given from the Bartholomew definition (Ref. [3]) :

$$f_{XL}(E_i, E_\gamma, \pi_i, J_i) = a_{XL} < B_{XL}(E_i, E_\gamma, \pi_i, J_i) > \rho(E_i) \tag{11}$$

With $< B_{XL}(E_i, E_\gamma, \pi_i, J_i) >$ being the mean over the excitation energies of reduced probability element in a bin of E_γ and $\rho(E_i)$ the density of state at the given excitation energy. The constant a_{XL} depends on the transition. The values used in this work are given in the Table 4.3. As seen in this table, the magnetic dipole transitions ($M1$) are usually much smaller in magnitude compared to the electric dipole transitions. However, at low E_γ, because they preserve parity while $E1$ is a parity changing transition, they may dominate. $E2$ transitions yields even smaller transitions at low energy

Table 2: Table of the coupling constants used in RSF codes

	E1 (e^2fm^2)	M1 (μ_N^4)	E2 (e^2fm^4)
a_{XL}	$1.04 \cdot 10^{-6}$	$1.158 \cdot 10^{-8}$	$0.80632 \cdot 10^{-12}$

they might have relevance like $M1$ transitions because they also are parity-preserving transitions. In the present work, we shall use B and LD values obtained within the shell model framework.

4.4 Brink-Axel's hypothesis

This is the assumption the photoabsorption cross section does not depend on the properties of the initial state, this means that the RSF should not depend on the energy or the spin of the initial state. The consequence that lies beneath is that the absorption RSF built on an excited state can be approximated by the one built on the ground state.In that case, the Brink's hypothesis is equivalent to : $\overrightarrow{f} = \overleftarrow{f} = f$. This is a strong assumption and as such its validity can be questioned. Experiments have shown that the hypothesis is fulfilled in good approximation for the giant dipole resonance region. The deviations from the hypothesis have been observed for low transition energies by Refs. [14] and [12].

4.5 Towards this work

As stated previously, RSF have been computed previously for $M1$ transitions for multiple isotopes of chromium and titanium in Ref. [13]. $E2$ transitions have been studied previously for heavier elements, namely ^{94}Mo and ^{95}Mo in Ref. [14]. This work will focus on $E2$ transitions for ^{48}Cr, ^{48}Ti and ^{50}Ti and comparing them to $M1$ transitions for theses elements. These elements can be studied in the pf shell and as such, there is only the positive parity to consider. For each nucleus, 600 states for spin going from 0 to 12, 41130 $M1$ transitions and 63130 $E2$ transitions have been previously computed using Large-Scale Shell Model (LSSM) code at the IPHC as shown in Ref. [17]. These will be the so-called input files which are used in the code presented in the following section.

5 Results

5.1 Code

To study the RSF a python code was developed during this internship.This code used two kind of files. The first are the spectrum files, which yields most notably, the spin of the nucleus, the parity, the excitation energy and the energy state. There is a spectrum files for each parity. The second are the transitions files, which are encoding the transitions calculations done in the Large-Scale Shell Model (LSSM). Whether the transition changes parity such as in E1 or not, there is one file or two files, respectively. They yield the initial spin, the final spin, the energy of the state, the energy of the γ-transition, the reduced probability transition, denoted as $BXL(J_i -> J_f)$ and the $BXL(J_f -> J_i)$. When the calculations are done in the LSSM, the states are not sorted by their excitation energies, thus we have a mix of upward and downward transitions so we need to sort them to have only downward transitions (deexcitations). As such, when a negative transition energy is encountered, this means we have an upward transition so we need to exchange the initial and final states to have a downward transition.
The spectrum files are used to compute the level density as a function of the excitation energy, whether it is the total LD or the LD by spin. The transition files are used to compute the averages of the reduced probability transition as a function of the E_γ. The code lets the user choose the element of interest, the type, the multipolarity, the bin width, whether cuts in the excitation energy are wanted or not and to choose between different plots. It is also possible to select transitions corresponding to the yrast bands.
Another code has been written to retrieve, for a given set of transitions, between which states the transitions do occur, and their associated configurations. $E2$ transitions have not been previously studied, except for [14] which was a study of ^{94} Mo and ^{95} Mo which would be our main comparison point.

5.2 Yrast bands

The yrast level schemes for the three nuclei of interest have been represented on Fig. 5. Depending

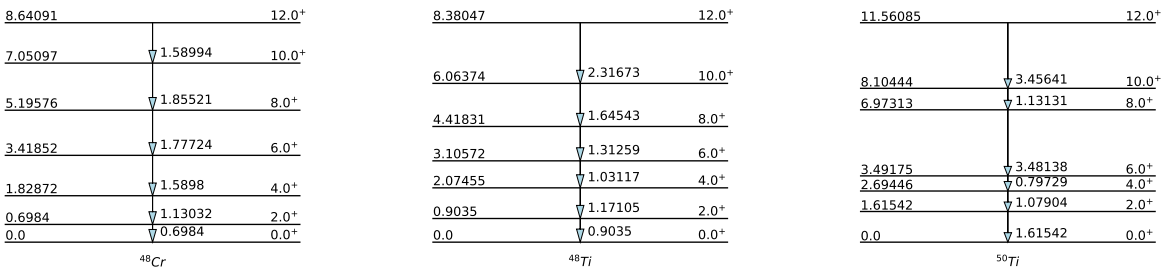

Figure 5: The levels scheme for the yrast of the three nuclei. The gap in excitation energy between two consecutives levels have been noted near the arrows. The excitation energy is in MeV.

on the spacing and the law followed by the levels scheme, one can determine the shape of a nucleus. If the nucleus is spherical, the energy of its levels follows a law $E_n = n\hbar\omega$ with n a natural number, whereas if the nucleus is deformed then it follows a law in $E = J(J+1)/\mathcal{J}$ where J is the spin and $\mathcal{J}$ is the moment of inertia of the nucleus.
The 2^+ level is much higher in ^{50}Ti than it is in ^{48}Cr and ^{48}Ti which is typical of a closed-shell nucleus (in this case, it has 28 neutrons, which is a magic number) and as such, of a spherical nucleus. ^{48}Ti levels are more evenly spaced which tends to confirm that this nucleus is not deformed whereas ^{48}Cr is.
The yrast band for the ^{48}Cr has been previously studied in Ref. [17] where different theoretical calculations using the Shell Model with the KB3 interaction, the Gogny Force and the cranked Hartree-Fock-Bogoliubov have been compared to experimental data. A good rotor must have a nearly constant Q_0, which is the case up to $J = 10$ in ^{48}Cr after which it is shown to backbend as seen on [17].

5.3 RSF of $M1$ and $E2$ transitions

The RSF have been presented in Sec. 4.3. The yielded results for each nucleus and for both transitions types are plotted on Fig. 6. As we can see, the strength function of $M1$ is much higher than the

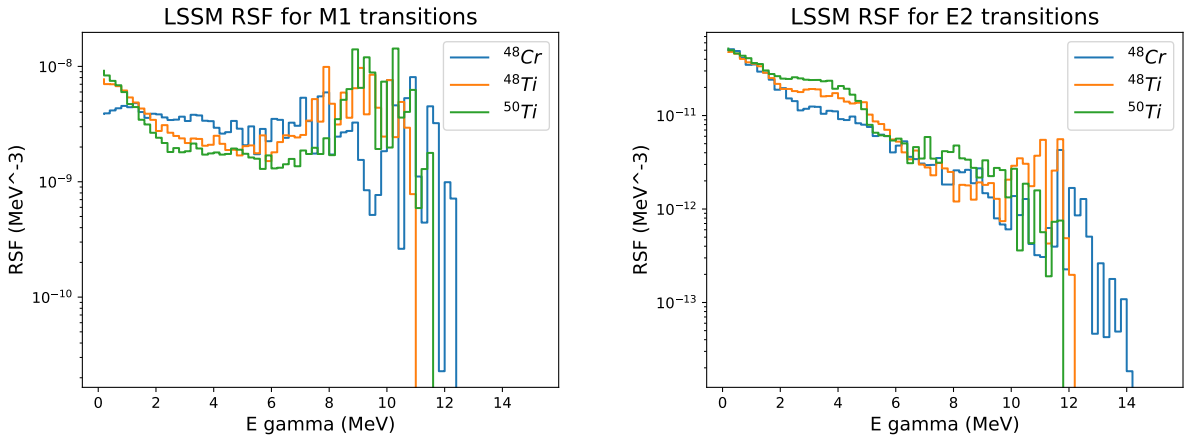

Figure 6: The RSF for $E2$ and $M1$ transitions obtained from shell-model calculations.

strength of $E2$ for each nucleus. Most notably, while there is an enhancement at low-energies for ^{48}Ti and ^{50}Ti, there is no such enhancement for ^{48}Cr. On the contrary, there is such an enhancement for both nuclei in $E2$ transitions. Enhancement of $M1$ transitions have been reported in the literature such as for ^{44}Sc in [11]. For the two titanium nuclei, there is an increase of the RSF which comes directly from the increase of the $B(M1)$ for $E_\gamma > 6$ MeV. This increase is less prominent and does not appear after $E_\gamma > 8$ MeV. In the case of $E2$, there is no such increase in $B(E2)$, hence the decrease of the corresponding RSF with the increase of E_γ.
As discussed previously in 4.2.2, the increase of the low-energy RSF can be due to a phenomenon called magnetic rotation. This effect has been predicted to appear in different regions of nuclei, as can be seen in Fig. 7 taken from [4].

From this figure we can see the two titanium nuclei are indeed in a region where the magnetic rotation has been predicted to be possible whereas it is not the case for ^{48}Cr, which is in accordance with the finding of a low energy enhancement or not in the nuclei of this study. Magnetic rotation has been previously proposed as an explanation of the increase of the RSF for nuclei in Ref. [14].
Finally, $M1$ transitions yield a RSF of around 2 orders of magnitude higher than $E2$ transitions. As such, $E2$ transitions can be neglected in comparison to $M1$ transitions. Even for the ^{48}Cr where there is no enhancement at low energies, the $M1$ transitions remains 10 times higher than the highest $E2$ transitions for this element which are at $E_\gamma \approx 0$ MeV.

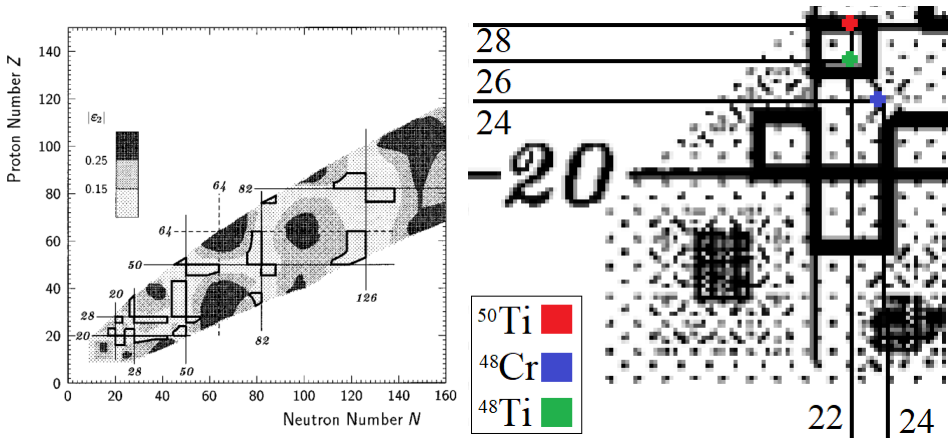

Figure 7: On the left : predicted mass regions where magnetic rotation is possible. These regions are enclosed by thick solid lines ; on the right : zoom on the nuclei of this work

5.4 Testing the Brink-Axel's hypothesis

This hypothesis has been discussed in Sec. 4.4. We can ascertain its validity by studying the behavior of the RSF obtained with different cuts in excitation energy, as shown on Fig. 8. If this hypothesis holds true, then the RSF should remain the same independently of the applied cuts in excitation energies. For each nucleus and for the two types of transitions, we can see that the RSF done using states in the range $0-8$ MeV and $5-8$ MeV are identical. This is due to the dominance of the high energy states in the RSF. We can note that for ^{48}Cr, there is a drop in the $E2$ RSF for E_γ in the range $1-5$ MeV in the excitation energy range $4-6$ MeV, which is not the case for the $M1$ RSF and the $E2$ RSF of the two titanium nuclei.
Besides, the behavior at low energies is preserved regardless of the cuts applied in excitation energies. We still have the enhancement for $E2$ transitions at low energies for each of the nuclei. Also, there is still an enhancement for $M1$ transitions at low energies for the two titanium nuclei while there is no such enhancement for the chromium. All in all, we can consider that the Brink-Axel hypothesis tends to be well respected.

5.5 Spin-flip

The previous RSF have been computed by performing an average over the spins a the partial RSF, ie. the RSF for a given spin. These partial RSF are represented on Fig. 9. This is an another mean to test the correctness of the Brink-Axel's hypothesis as it an other way to see this independence of the RSF with respect to the properties of the initial state. In fact, looking for the independence of spins rather than the independence of the excitation energy is an even stronger statement.
For $M1$ transitions, the 0^+ states are contributing a bit more than the other states. Around $6-8$ MeV, we can see an increase of the RSF strength function. This is called the spin-flip which are transitions between single-particle states which have especially strong $M1$ matrix element. These transitions have the same l but different j. Here this spin-flip occur between $f7/2$ and $f5/2$ state. Due to the energetical gap at $N = 28$, a lot of energy is needed to promote a particle to the $f5/2$ orbital hence the apparition of this structure around 6 MeV.
In the case of $E2$ transitions, we can note that the partial RSF of $J = 0^+$ is especially strong when compared to the RSF for the other spins. They are strongly coupled with 2^+ hence $2^+ \rightarrow 0^+$ yields the major contributions to the RSF.
Also, there are peaks of RSF values around $1-3$ MeV for the ^{48}Cr. While peaks do appear in ^{48}Ti and ^{50}Ti, they occur at higher energies, at $4-6$ MeV.

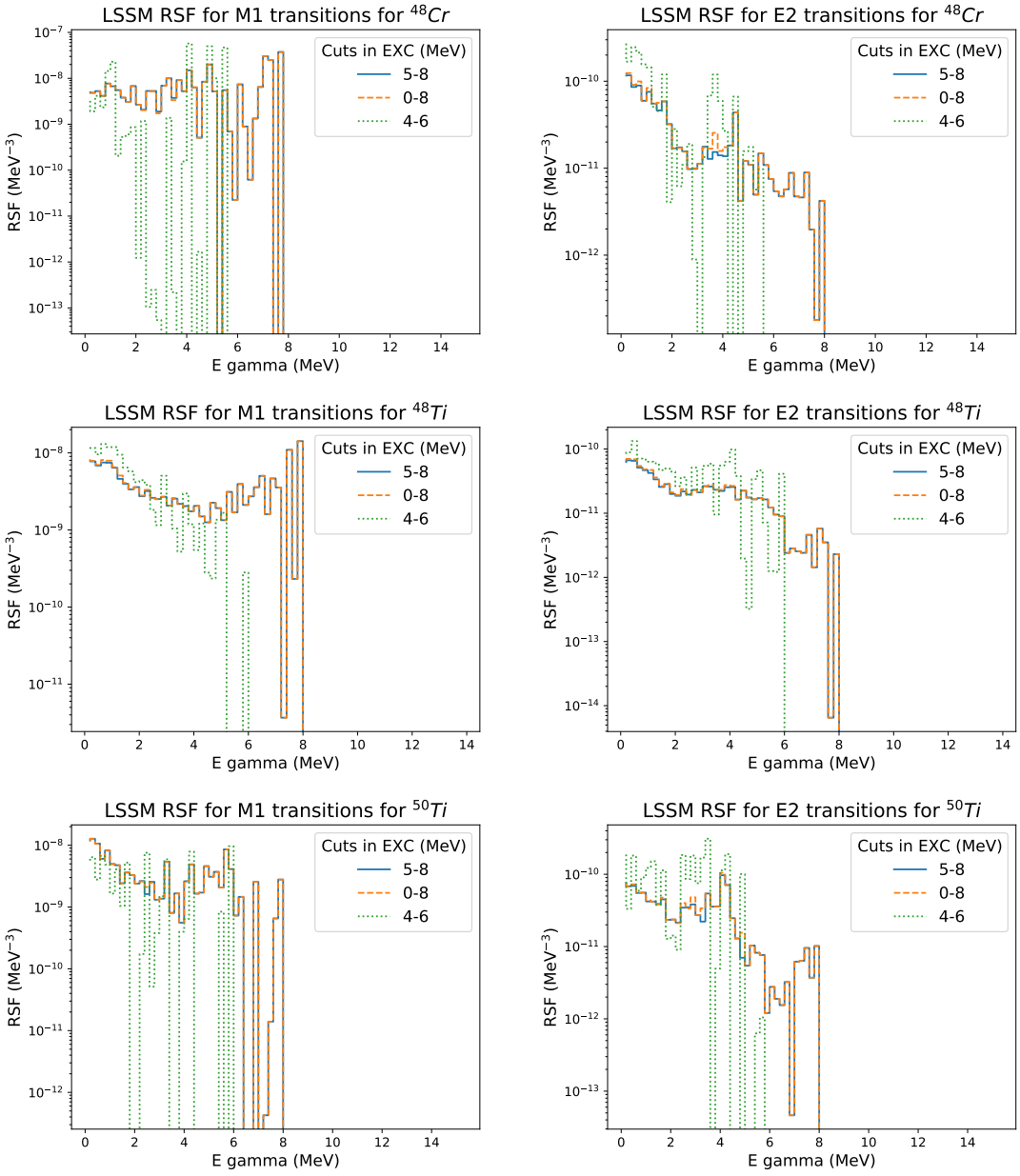

Figure 8: Plots of the $M1$ and $E2$ RSF for different cuts in excitation energy for the nuclei ^{48}Cr, ^{48}Ti and ^{50}Ti

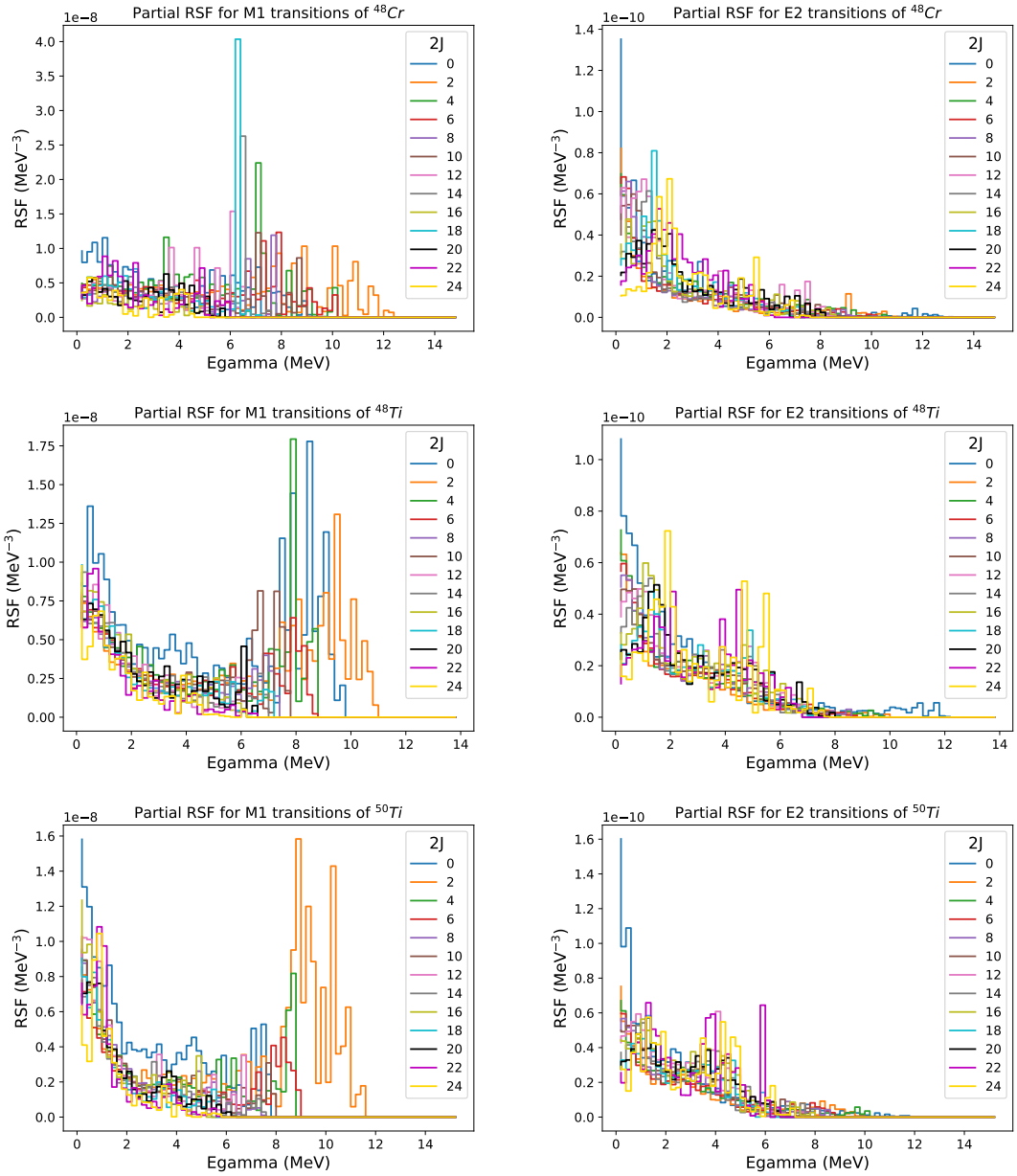

Figure 9: Partial $M1$ and $E2$ RSF for the nuclei ^{48}Cr, ^{48}Ti and ^{50}Ti

5.6 Main contributions

For $E2$ and $M1$ RSF, we can study which transition yield the greatest $B(E2)$ (respectively $B(M1)$) value at low energies (under $E_\gamma = 2$ MeV) in a given energy bin. We have taken a bin of 0.2 MeV. This enables us to look at which states yield the strongest transition. We can extend the definition of the greatest value to all the B value which have at least 90% of the maximum, but this does not yield many more states. As such we will concentrate each time only on the strongest transition.
For ^{48}Cr, the states yielding the major contributions for $E2$ are mostly with 4 protons and 4 neutrons on the $f7/2$ shell for both the initial state and the final state. Those states also have minor contributions of states with 3 proton and/or 3 neutrons in the $f7/2$ and 1 proton and/or 1 neutron in the $p1/2$ shell. The transitions found are mostly of the kind of $J_f = J_i - 2$ except at very low energies (ie. the first two bins) where it is $J_f = J_i - 1$. Concerning $M1$ transitions, the states found are essentially the same albeit most of the transitions occur between states with $J_f = J_i - 1$.
Concerning ^{50}Ti the $E2$ transitions found are connecting states with $J_f = J_i - 1$ in the range $0 < E_\gamma < 1$ while the transitions in the range $1 < E_\gamma < 2$ are connecting $J_f = J_i - 2$. Theses stares are mostly states with the two protons on the $f7/2$ shell for both the initial and the final state. For the neutrons, those states mostly corresponds to states with 6 or 7 neutrons on the $f5/2$ and 2 or12 on the $p1/2$. There also some states where one of the configurations presents 2 neutrons on the $p3/2$ shell or other mixing between the 4 uppermost shells. For $M1$ transitions, the states connected are also dominated by states with 2 protons on the $p7/2$ shell and 6 or 7 neutrons on the $f5/2$ and 2 or1 on the $p1/2$. The connected states are states with $J_f = J_i - 2$
The same study was done for ^{48}Ti where the states yielding the largest $B(M1)$ have been found to occur between states where $J_f = J_i, J_i \pm 1$. The dominating states are with 2 protons in the f7/2 shell or with one proton in the f7/2 shell and one in the p1/2. The 6 neutrons are in the f7/2 state. The higher the energy goes and the more other configurations appears for the neutrons. There are configurations with 4 neutrons in the f5/2 shell and the 2 remaining in the p3/2 shell and configurations with 4 neutrons in the f7/2, 1 neutron in the p3/2 shell and the last neutron being in a lower shell, not in the 4 upper shells. The largest $E2$ transitions are essentially connecting $J_f = J_i, J_i \pm 1$ for $0 < E_\gamma < 1$ while they are connecting $J_f = J_i, J_i \pm 2$ for $E_\gamma > 1$ MeV.
In comparison Ref.[14] has found that the transitions occurs between states with $J_f = J_i, J_i \pm 1$. Notably, these transitions have been shown to occur between states yielding large $B(M1)$ values. In this study, it was found that both the large $B(M1)$ values in ^{48}Ti and the large $B(E2)$ values in ^{48}Cr were also connecting states with $J_f = J_i, J_i \pm 1$. However, it was found for ^{50}Ti that the transitions yielding the large $B(E2)$ values were connecting states with $J_f = J_i - 2$. In Ref. [14] it was found that instead of having an exponential rise near the lower energies, the LSSM predicts a finite maximum of a Gauss-like shape. Here the increase at lower energies predicts more a linear slope which *in fine* leads to a finite maximum. In fact this can be a Gauss-like shape which would more widened than in Ref. [14].

6 Conclusions and perspectives

This work has used previously computed diagonalization of the nuclear hamiltonian to study the properties of the RSF of two types : $E2$ and $M1$ in three nuclei : ^{48}Cr, ^{48}Ti and ^{50}Ti. That leads to a comparative analysis between $M1$ and $E2$ transitions in each of the aforementioned elements. There is an enhancement at low energies for ^{48}Ti and ^{50}Ti but not for ^{48}Cr in $M1$ transitions while there is such an enhancement for $E2$ transitions for the three nuclei. This can be explained by the shape of the nucleus, because the ^{48}Cr is not spherical whereas the two others are. The calculations of the RSF are done under the Brink-Axel's hypothesis, which is better fullfilled for the RSF of the two types in the ^{48}Ti and ^{50}Ti than in ^{48}Cr. It has been found that in spite of the low-energy structure effects found in $E2$ strength functions and regarding possible deviations from the phenomenological formula predicted in RIPL as in the case of Ref. [14], their magnitude is much smaller than in the $M1$ strength functions, so it seems the $E2$ can be disregarded in microscopic calculations of the RSF even in well deformed nuclei like ^{48}Cr. For each nucleus and for the two type of transitions, the main configurations have been found at low energies. A microscopic study of the structure effects for these

elements could be performed next to probe appearing structure effects.
I acknowledge Kamila Sieja for her availability which yields me quick answers despite the epidemic.

References

[1] Loens, Hans Peter. Microscopic radiative strength functions and fission barriers for r-process nucleosynthesis. Germany: PhD thesis, TU Darmstadt, 2011

[2] D.Rochman *et al.*, Phys. Lett. B (2016).

[3] G.A. Bartholomew, E.D. Earle, A.J. Ferguson, J.W. Knowles, and M.A. Lone. Adv. Nucl. Phys., 7:229, 1972.

[4] S. Frauendorf, Rev. Mod. Phys. 73, 463

[5] K.S. Krane,Introductory Nuclear Physics (Wiley, New York/Chichester/Brisbane/Toronto/Singapore) (1988).

[6] in Proceedings of the Workshop on Gamma Sphere Physics, Berkeley, edited by M.A. Deleplanque, I.Y. Lee, and A.O. Macchiavelli (World Scientific, Singapore), p. 272.

[7] S. Goriely, S. Hilaire, S. Péru, M. Martini, I. Deloncle, and F. Lechaftois, Phys. Rev. C 94, 044306 (2016)

[8] S. Goriely, S. Hilaire, S. Péru and K. Sieja, Phys. Rev. C 98, 014327 (2018)

[9] R. Schwengner, S. Frauendorf, and A. C. Larsen, Low-Energy Enhancement of Magnetic Dipole Radiation, Phys. Rev. Lett., 118:092502, 2013

[10] A. C. Larsen, J. E. Midtbø, M. Guttormsen, T. Renstrøm, S. N. Liddick, A. Spyrou, S. Karampagia, B. A. Brown, O. Achakovskiy, S. Kamerdzhiev, D. L. Bleuel, A. Couture, L. Crespo Campo, B. P. Crider, A. C. Dombos, R. Lewis, S. Mosby, F. Naqvi, G. Perdikakis, C. J. Prokop, S. J. Quinn, and S. Siem. Phys. Rev. C, 97:054329, May 2018.

[11] K.Sieja, Phys. Rev. Lett. 119, 052502 (2017)

[12] K.Sieja, Phys. Rev. C 98, 064312 (2018)

[13] K.Sieja & S. Goriely Recent shell-model calculations of gamma-decay strength functions, to appear in Acta Physics Polonica (2020)

[14] R. Schwengner, Phys. Rev. C 90,064321 (2014)

[15] https://www-nds.iaea.org/RIPL-3/

[16] E. Caurier, A. P. Zuker, A. Poves, and G. Martínez-Pinedo,Phys. Rev. C 50, 225 (1994)

[17] E. Caurier, G. Martínez-Pinedo, F. Nowacki, A. Poves, and A. P. Zuker, Rev. Mod. Phys. 77, 427 (2005)